

<sup>13</sup>M. S. Chen, I. J. Muzinich, H. Terazawa, and T. P. Cheng, Phys. Rev. D **7**, 3485 (1973).

<sup>14</sup>See, e.g., discussion in Ref. 1, pp. 161 and 162.

<sup>15</sup>D. M. Scott, Nucl. Phys. **B49**, 99 (1972).

<sup>16</sup>We note that although we have used  $(\ln s)$  in our work, assuming reasonable values of  $\tau$ , at low values of  $\tau$ , where much measurement may be made, the suppression of  $W_3$  in the Drell-Yan term is in fact  $O((q^2)^{-1})$ ,

and the suppression factor in the diffractive term is a power of  $(\ln q^2)$  rather than of  $(\ln s)$ . See note in P. V. Landshoff and J. C. Polkinghorne, Nucl. Phys. **B36**, 642 (1972).

<sup>17</sup>J. L. Cardy and G. A. Winbow, Phys. Lett. **52B**, 95 (1974).

<sup>18</sup>C. E. DeTar, S. D. Ellis, and P. V. Landshoff, CERN Report No. TH. 1925, 1974 (unpublished).

## Probing parton distribution functions in massive lepton-pair production\*

Gilbert Chu

*Lawrence Berkeley Laboratory, University of California, Berkeley, California 94720*

John F. Gunion

*Department of Physics, University of Pittsburgh, Pittsburgh, Pennsylvania 15213*

(Received 20 June 1974)

We analyze massive  $\mu$ -pair production in hadron-hadron collisions using the parton model, and obtain expressions for general differential cross sections,  $d\sigma/d^4Q$ , in the  $\mu$ -pair momentum. We indicate ways in which the parton distributions in both longitudinal and transverse momenta may be probed in detail. Finally, we apply our results to the data by using parton distribution functions with threshold behavior ( $\omega = 1/x \rightarrow 1$ ) implied by the interchange model for large-angle scattering. Our results are that (1) the calculated cross section is only five percent of the observed cross section at Brookhaven energies; (2) inclusion of nonpointlike structure for the partons which enables one to explain the  $e^+e^-$  annihilation data results in only a marginal improvement in the normalization, but (perhaps accidentally) allows one to approximately describe the shape of the invariant mass distribution  $d\sigma/dQ^2$ .

### INTRODUCTION

The ability of the parton model<sup>1</sup> to "explain" the apparent scaling of the electroproduction data in the SLAC-MIT experiments<sup>2</sup> does not in itself provide conclusive evidence for such a composite hadronic picture. Theories based on vector-meson dominance<sup>3</sup> and, indeed, any models with appropriate light-cone behavior<sup>4</sup> are viable alternatives.

The importance of extracting and experimentally testing predictions of the parton model for other processes is manifest. Particularly important examples are electron-positron annihilation,<sup>5</sup> high-transverse-momentum reactions,<sup>6</sup> and massive  $\mu$ -pair production.<sup>7-9</sup> The existing  $e^+e^-$  annihilation data<sup>10,11</sup> are not easily interpreted within the parton framework without modifications to the pointlike structure of the partons.<sup>12</sup> On the other hand, high-transverse-momentum phenomena seem to lend considerable support to parton-model ideas.<sup>6</sup>

Indeed there is a definite consistency between deep-inelastic and high- $p_{\perp}$  processes. The wave functions<sup>13,14</sup> describing the breakup of a hadron

into partons, suggested by the interchange and dimensional counting models of high-transverse-momentum interactions, seem to be in remarkable agreement with the deep-inelastic data. Of particular importance is the very different behavior of parton vs antiparton distribution functions. This difference leads to substantial alterations in the expectations of the parton model for the, as yet, incompletely measured cross section for massive  $\mu$ -pair production. A rough treatment of these alterations was given in Ref. 14. In this paper we shall employ the more precise distribution functions of Ref. 13 to analyze the  $\mu$ -pair production data in detail.

We shall also prepare a largely kinematical modification of the traditional analysis which is vital in making reliable parton-model predictions at subasymptotic energies. We give a method for taking account of the phase-space limitations of the  $\mu$ -pair invariant mass squared up to order  $\sqrt{s}$ . At the energies of the Brookhaven-Columbia experiment<sup>15</sup> the modifications are substantial.

Finally, we shall discuss the importance of mea-

asuring the longitudinal *and* transverse momentum distributions of the  $\mu$  pair. In particular, a definite correlation between the transverse and longitudinal momentum distributions is expected as the edge of phase space is approached.

I. KINEMATICS AND CROSS-SECTION FORMULAS

We first discuss the necessary corrections to and amplifications of the asymptotic cross-section formulas contained in the literature.<sup>7</sup> It is convenient and perhaps interesting to use a slightly different technique for deriving the results. Neither naive parton-model calculations nor the relatively more complicated Sudakov analysis<sup>16</sup> need be employed.

The invariant cross section for production of a massive  $\mu$  pair (Fig. 1) may be written as

$$d\sigma = \frac{1}{[\lambda(s, M_1^2, M_2^2)]^{1/2}} \frac{4\pi\alpha^2}{3Q^2} \frac{d^4Q}{(2\pi)^4} W_{\mu}^{\mu}(p_1, p_2, Q), \tag{1.1}$$

where we have neglected the lepton masses, and where  $p_1, p_2,$  and  $Q$  are the two initial hadron momenta and final massive  $\mu$ -pair total momentum

$$W^{\mu\nu}(p_1, p_2, Q) = \sum_a \frac{\lambda_a^2}{(2\pi)^4} \int d^4k_1 d^4k_2 \delta^4(k_1 + k_2 - Q) \text{Tr}[T_a(p_1, k_1)\gamma^{\mu}T_{\bar{a}}(p_2, k_2)\gamma^{\nu}], \tag{1.3}$$

where the parton charge is given by  $\lambda_a e$ . The summation extends over all species,  $a$ , of partons and antipartons. The index  $\bar{a}$  refers to the antiparticle of  $a$ . We perform the integrations of (1.3) in the special frame:

$$\begin{aligned} p_1 &= \left( P + \frac{M^2}{4P}, \vec{0}_{\perp}, P - \frac{M^2}{4P} \right), \\ p_2 &= \left( P + \frac{M^2}{4P}, \vec{0}_{\perp}, -P + \frac{M^2}{4P} \right), \\ k_1 &= \left( x_1 P + \frac{k_{1\perp}^2 + k_{1\perp}^2}{4x_1 P}, \vec{k}_{1\perp}, x_1 P - \frac{k_{1\perp}^2 + k_{1\perp}^2}{4x_1 P} \right), \\ k_2 &= \left( x_2 P + \frac{k_{2\perp}^2 + k_{2\perp}^2}{4x_2 P}, \vec{k}_{2\perp}, -x_2 P + \frac{k_{2\perp}^2 + k_{2\perp}^2}{4x_2 P} \right), \\ Q &= [(Q^2 + y^2 P^2 + Q_{\perp}^2)^{1/2}, \vec{Q}_{\perp}, yP], \end{aligned} \tag{1.4}$$

where  $y$  is the longitudinal momentum fraction of  $Q$  in the center-of-mass system. Though  $P$  is of order  $(s/2)^{1/2}$ , it should be stressed that this is not an infinite-momentum frame. The parton integration volume is, up to order  $1/s$ ,

$$d^4k_i = \frac{dx_i}{2|x_i|} d^2k_{i\perp} d(k_i^2) + O\left(\frac{1}{s}\right). \tag{1.5}$$

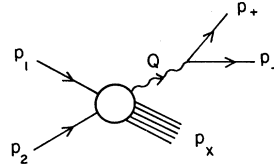


FIG. 1. Kinematics for  $pp \rightarrow \mu^+\mu^- + \text{anything}$ .

$$W^{\mu\nu}(p_1, p_2, Q) = (2\pi)^6 2E_1 2E_2 \int d^4x e^{-iQ \cdot x} \times \langle p_1 p_2 | j^{\mu}(x) j^{\nu}(0) | p_1 p_2 \rangle. \tag{1.2}$$

According to the parton-model picture originally proposed by Drell and Yan<sup>7</sup> the massive photon arises via parton-antiparton annihilation (Fig. 2). For general interest and in order to be certain of including nonasymptotic phase-space effects we will recalculate the annihilation diagram in a special frame.

Denote the parton-hadron forward scattering amplitude, averaged over hadron spins, by  $T_a(p_i, k_i)$  for a parton of type  $a$ . Note that  $T_a$  is a matrix in the parton spinor indices. The contribution of Fig. 2 to  $W^{\mu\nu}$  is

As in Ref. 16, we write a dispersion relation for  $T_a$

$$T_a(p_i, k_i) = \int d\sigma_i \frac{\rho_a(p_i, k_i, \sigma_i)}{(p_i - k_i)^2 - \sigma_i + i\epsilon}. \tag{1.6}$$

In the above frame

$$\begin{aligned} \rho_a(p_i, k_i, \sigma_i) &= \frac{1}{\pi} \text{Im} T_a(p_i, k_i) \Big|_{(p_i - k_i)^2 = \sigma_i}, \\ s_i &\equiv (p_i - k_i)^2 \\ &= (1 - x_i)M^2 - \frac{(1 - x_i)}{x_i} k_{i\perp}^2 - \frac{1}{x_i} k_{i\perp}^2 + O\left(\frac{1}{s}\right). \end{aligned} \tag{1.7}$$

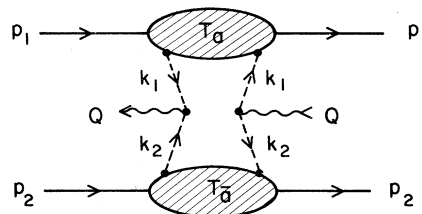


FIG. 2. Parton-antiparton annihilation diagram.

For  $x_i$  in the interval  $(0, 1)$ , one may perform the  $k_i^2$  integrations by picking up the pole in  $s_i$  as shown in Fig. 3. [For  $x_i$  outside the interval  $(0, 1)$  the  $s_i$  and  $k_i^2$  singularities at  $\sigma_i - i\epsilon$  and  $\mu^2 - i\epsilon$

both lie in the lower half of the  $k_i^2$  plane. Thus the contour can be closed in the upper half plane giving a zero result.] The result can be written as

$$W^{\mu\nu}(p_1, p_2, Q) = \sum_a \frac{\lambda_a^2}{16\pi^2} \int_0^1 \frac{dx_1}{1-x_1} \frac{dx_2}{1-x_2} \int d^2k_{1\perp} d^2k_{2\perp} d\sigma_1 d\sigma_2 \delta^4(k_1 + k_2 - Q) \text{Tr}[\rho_a(p_1, k_1, \sigma_1) \gamma^\mu \rho_a^-(p_2, k_2, \sigma_2) \gamma^\nu], \quad (1.8)$$

where the  $k_i^2$  are now evaluated at

$$k_i^2 = x_i M^2 - \frac{k_{i\perp}^2}{1-x_i} - \frac{x_i}{1-x_i} \sigma_i + O\left(\frac{1}{s}\right). \quad (1.9)$$

In standard fashion, one decomposes each  $\rho_a$  into its various possible tensor forms,

$$\rho_a(p_i, k_i, \sigma_i) = V_a(k_i^2, \sigma_i) \not{p}_i + \tilde{V}_a(k_i^2, \sigma_i) \not{k}_i + [\text{terms which leave } O(1/s) \text{ corrections to } W^{\mu\nu}], \quad (1.10)$$

so that, neglecting the  $O(1/s)$  corrections,

$$W^{\mu\nu}(p_1, p_2, Q) = \sum_a \frac{\lambda_a^2}{16\pi^2} \int \frac{dx_1}{1-x_1} \frac{dx_2}{1-x_2} d^2k_{1\perp} d^2k_{2\perp} d\sigma_1 d\sigma_2 \times \delta^4(k_1 + k_2 - Q) 4(p_1^\mu p_2^\nu + p_2^\mu p_1^\nu - g^{\mu\nu} p_1 \cdot p_2) (V_a + x_1 \tilde{V}_a)(V_a + x_2 \tilde{V}_a). \quad (1.11)$$

In the present frame the above approximation is gauge invariant to order  $1/s$ . The functions  $V_a$  and  $\tilde{V}_a$  are simply related to the distribution functions measured in deep-inelastic scattering

$$f_a^k(x_i) = \frac{1}{8\pi^3} \int d\sigma_i d^2k_{i\perp} \frac{1}{1-x_i} [V_a^k(k_i^2, \sigma_i) + x_i \tilde{V}_a^k(k_i^2, \sigma_i)] \\ \equiv \int d\sigma_i d^2k_{i\perp} f_a^k(x_i, k_{i\perp}^2, \sigma_i), \quad (1.12)$$

where  $k$  denotes the hadron type. The deep-inelastic structure function for the colliding hadron is then given by

$$F_2^k(x=1/\omega) = \sum_a \lambda_a^2 x f_a^k(x). \quad (1.13)$$

Using (1.12) and (1.11) we obtain

$$d\sigma = \sum_a \frac{4\pi\alpha^2}{3Q^2} \lambda_a^2 \int \frac{d^4Q}{(2\pi)^4} dx_1 dx_2 d^2k_{1\perp} d^2k_{2\perp} d\sigma_1 d\sigma_2 (2\pi)^4 \delta(k_1 + k_2 - Q) f_a^1(x_1, k_{1\perp}^2, \sigma_1) f_a^2(x_2, k_{2\perp}^2, \sigma_2), \quad (1.14)$$

which, in the asymptotic limit  $s \rightarrow \infty$ , reduces in familiar fashion to

$$\frac{d\sigma}{dQ^2} = \sum_a \frac{4\pi\alpha^2}{3Q^2} \frac{\lambda_a^2}{Q^2} \int dx_1 dx_2 \delta(x_1 x_2 - Q^2/s) x_1 f_a^1(x_1) x_2 f_a^2(x_2). \quad (1.15)$$

Expressing (1.14) in terms of  $y$  (the fractional longitudinal momentum of the massive photon relative to that of the incoming hadron, 1), the variable  $\tau = Q^2/s$  and  $Q_{\perp}$ , we have as  $s \rightarrow \infty$

$$x_1 = \frac{+y + (y^2 + 4\tau + 4Q_{\perp}^2/s)^{1/2}}{2}, \\ x_2 = \frac{-y + (y^2 + 4\tau + 4Q_{\perp}^2/s)^{1/2}}{2}, \quad (1.16)$$

$$\vec{k}_{1\perp} + \vec{k}_{2\perp} = \vec{Q}_{\perp},$$

with  $-(1-\tau) < y < (1-\tau)$  and  $x_1$  and  $x_2$  in the interval  $(0, 1)$ :

$$\frac{d\sigma}{dy d^2Q_{\perp} d\tau} = \frac{1}{(y^2 + 4\tau + 4Q_{\perp}^2/s)^{1/2}} \sum_a \frac{8\pi\alpha^2}{3Q^2} \lambda_a^2 \int d^2k_{\perp} d\sigma_1 d\sigma_2 f_a^1(x_1, \vec{k}_{\perp}, \sigma_1) f_a^2(x_2, \vec{Q}_{\perp} - \vec{k}_{\perp}, \sigma_2). \quad (1.17)$$

Finally from (1.14) we can obtain the important subasymptotic corrections to the expression for  $d\sigma/dQ^2$ . These may be incorporated to order  $1/\sqrt{s}$  by replacing the  $\delta$  function of (1.15) by the full expression for  $s\delta((k_1+k_2)^2-Q^2)$  and exposing the  $k_{1\perp}$ ,  $k_{2\perp}$ ,  $\sigma_1$ , and  $\sigma_2$  integrations

$$s\delta((k_1+k_2)^2-Q^2) = \delta \left[ x_1x_2(1-2M^2/s) + (x_1+x_2)M^2/s - \frac{x_1\sigma_1}{(1-x_1)s} - \frac{x_2\sigma_2}{(1-x_2)s} - \frac{k_{1\perp}^2/s}{1-x_1} - \frac{k_{2\perp}^2/s}{1-x_2} - \tau \right]. \quad (1.18)$$

The frame (1.4) thus allows us to ascertain that the naive result in (1.15) will only apply so long as  $1/(1-x_1)$  and  $1/(1-x_2)$  are not of order  $\sqrt{s}$ . In fact, we find from (1.18) that the maximum  $Q^2$  value occurs for  $x_1=x_2=1-M/\sqrt{s}$ ,  $\sigma_1=\sigma_2=M^2$  (the dispersion integral thresholds), and  $\vec{k}_{1\perp}=\vec{k}_{2\perp}=0$

$$Q^2_{\max} \cong s - 4M\sqrt{s} \cong (\sqrt{s} - 2M)^2.$$

Thus, we see that the threshold region,  $Q^2$  near  $Q^2_{\max}$ , probes parton-distribution functions near *their* threshold,  $x \sim 1$ , in a particularly sensitive fashion. We shall have more to say about this later.

## II. PROBING THE DETAILED BEHAVIOR OF QUARK DISTRIBUTION FUNCTIONS

The Columbia-Brookhaven collaboration has reported data on  $\mu$ -pair production between 22 and 29.5 GeV/c laboratory momentum, with  $Q^2 > 1$  (GeV/c)<sup>2</sup>.<sup>15</sup> However, there are as yet no data at sufficiently high energy, for the same  $\tau$  range, to provide an adequate test of the scaling behavior of  $d\sigma/dQ^2$ .

What can be done is to compare the parton model to the shape of the experimental distribution in  $d\sigma/dQ^2$  over the limited range of available energies. Such fits have been given in the past. However, the parton-distribution functions employed are now known to be too naive.<sup>13,14</sup> We shall repeat this type of analysis employing distribution functions<sup>13</sup> based on an examination of deep-inelastic scattering data and on theoretical considerations from the parton interchange model for large-angle scattering.

The distribution functions in the quark model are written in terms of valence  $\hat{u}$ , Regge  $r$ , and sea  $s$ , components

$$\begin{aligned} u_\phi(x) &= \hat{u}_\phi(x) + s(x) + r_\phi(x), \\ u_{\mathcal{N}}(x) &= \hat{u}_{\mathcal{N}}(x) + s(x) + r_{\mathcal{N}}(x), \\ u_{\bar{\phi}}(x) &= u_{\bar{\mathcal{N}}}(x) = s(x), \\ u_\lambda(x) &= u_{\bar{\lambda}}(x) = s'(x). \end{aligned} \quad (2.1)$$

We have incorporated the usual restrictions of duality. The distributions  $s(x)$  and  $r(x)$  are associated with the higher quark number, nonvalence states within the proton. The results of the theoretically motivated wave-function extraction are

$$\begin{aligned} \bar{s}(x) &\equiv \frac{5}{18} s(x) + \frac{1}{6} s'(x) \\ &= 0.2(1-x)^7/x, \\ r_\phi(x) &= 1.888(1-x)^7/x^{1/2}, \\ r_{\mathcal{N}}(x) &= 1.028(1-x)^7/x^{1/2}. \end{aligned} \quad (2.2)$$

The valence quark distributions,  $\hat{u}_\phi(x)$  and  $\hat{u}_{\mathcal{N}}(x)$ , are extracted from the SLAC-MIT data<sup>2</sup> by subtracting out the sea and Regge contributions, while demanding the satisfaction of the standard quantum-number sum rules:

$$\int (\hat{u}_\phi + r_\phi) dx \approx 2, \quad (2.3)$$

$$\int (\hat{u}_{\mathcal{N}} + r_{\mathcal{N}}) dx \approx 1. \quad (2.4)$$

It is found that

$$\hat{u}_{\mathcal{N}}(x) = 0.7(1-x)\hat{u}_\phi(x). \quad (2.5)$$

For  $x > 0.35$ ,  $\hat{u}_\phi(x)$  is proportional to  $(1-x)^3$  as expected from the Drell-Yan-West (DYW) relation,<sup>18</sup> and as  $x \rightarrow 0$ ,  $\hat{u}_\phi(x)$  vanishes, as expected theoretically.<sup>13</sup>

The above results may be partially understood as follows. (See Refs. 13 and 14 for details.) The higher threshold damping of the sea and Regge components,  $s(x)$  and  $r(x)$ , is that expected for a state of the proton with at least one extra  $q\bar{q}$  pair in addition to the usual three valence quarks. Such a state's contribution to the form factor of the proton at large momentum transfer is, in simple theories, proportional to  $1/t^{n-1}$ , where  $n$  is the num-

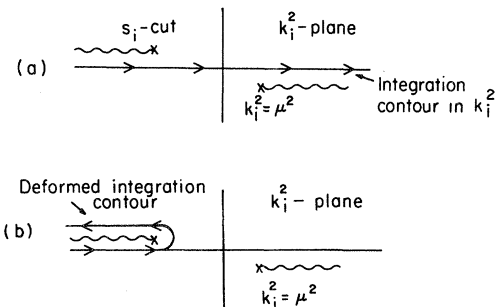


FIG. 3. (a) The  $k_i^2$ -plane singularities of  $T_a(s_i, k_i^2)$  when  $0 < x_i < 1$ , and the  $k_i^2$  integration contour. (b) The deformed contour.

ber of quarks and antiquarks. The DYW relation then associates a threshold damping of  $(1-x)^{2n-3}$  with this state. The present case has  $n=5$  ( $qqq\bar{q}q$ ). The  $1/x$  and  $1/x^{1/2}$  behaviors near  $x=0$  of  $s$  and  $r$  respectively are simply the standard Pomeron and Regge behaviors. The relation between  $\hat{u}_\phi$  and  $\hat{u}_{\mathfrak{N}}$  indicates a certain amount of  $\phi$ - $\mathfrak{N}$  quark pairing within the proton which results in  $F_2^{en}/F_2^{ep} \rightarrow \frac{1}{4}$  as  $x \rightarrow 1$ .

The neutrino data from Gargamelle<sup>19</sup> imply additional constraints for the fractional momentum carried by the various quarks

$$\int (u_\phi + u_{\bar{\phi}} + u_{\mathfrak{N}} + u_{\bar{\mathfrak{N}}}) dx = 0.49 \pm 0.07, \tag{2.6}$$

$$\frac{\int (u_{\bar{\phi}} + u_{\bar{\mathfrak{N}}} + u_{\bar{\lambda}}) dx}{\int (u_\phi + u_{\bar{\phi}} + u_{\mathfrak{N}} + u_{\bar{\mathfrak{N}}} + u_\lambda + u_{\bar{\lambda}}) dx} = 0.10 \pm 0.03.$$

These sum rules are also satisfied by the quark distributions of Ref. 13. Figure 4 displays the quark distribution functions.

For asymptotic energies, the  $\mu$ -pair production cross section measures a quadratic sum of quark distribution functions (see 1.17)

$$\begin{aligned} \Delta &\equiv \sum_a \lambda_a^2 f_a(x_1, \vec{k}_\perp) f_{\bar{a}}(x_2, \vec{Q}_\perp - \vec{k}_\perp) \\ &= \frac{12}{9} \bar{s}(x_1)_{\vec{k}_\perp} \bar{s}(x_2)_{\vec{Q}_\perp - \vec{k}_\perp} + \left\{ \frac{1}{9} [\hat{u}_{\mathfrak{N}}(x_1) + r_{\mathfrak{N}}(x_1)] + \frac{4}{9} [\hat{u}_\phi(x_1) + r_\phi(x_1)] \right\}_{\vec{k}_\perp} \bar{s}(x_2)_{\vec{Q}_\perp - \vec{k}_\perp} \\ &\quad + \bar{s}(x_1)_{\vec{k}_\perp} \left\{ \frac{1}{9} [\hat{u}_{\mathfrak{N}}(x_2) + r_{\mathfrak{N}}(x_2)] + \frac{4}{9} [\hat{u}_\phi(x_2) + r_\phi(x_2)] \right\}_{\vec{Q}_\perp - \vec{k}_\perp}, \end{aligned} \tag{2.7}$$

where

$$x_1 = \frac{y + (y^2 + 4\tau)^{1/2}}{2}$$

and

$$x_2 = \frac{-y + (y^2 + 4\tau)^{1/2}}{2},$$

with  $|y| < 1 - \tau$ . The subscripts denote transverse-momentum dependence.

A number of limits are of particular interest. (Reference 14 contains some of these results.) Consider  $y = 1 - \tau - \epsilon(1 + \tau)$  (i.e., near one of its kinematical limits). Then  $x_1 \cong 1 - \epsilon$ . Because of the strong threshold damping of  $s(x)$ , the surviving terms in  $\Delta$  yield

$$\begin{aligned} \Delta &\cong \left[ \frac{1}{9} \hat{u}_{\mathfrak{N}}(1 - \epsilon) + \frac{4}{9} \hat{u}_\phi(1 - \epsilon) \right] \bar{s}(\tau) \\ &\cong \epsilon^3 \bar{s}(\tau). \end{aligned} \tag{2.8}$$

For  $y=0$  and  $\tau \rightarrow 1$ ,  $x_1 = x_2 \rightarrow \tau$ , with the result

$$\begin{aligned} \Delta &\cong 2 \left[ \frac{1}{9} \hat{u}_{\mathfrak{N}}(\tau) + \frac{4}{9} \hat{u}_\phi(\tau) \right] \bar{s}(\tau) \\ &\cong (1 - \tau)^{10}. \end{aligned} \tag{2.9}$$

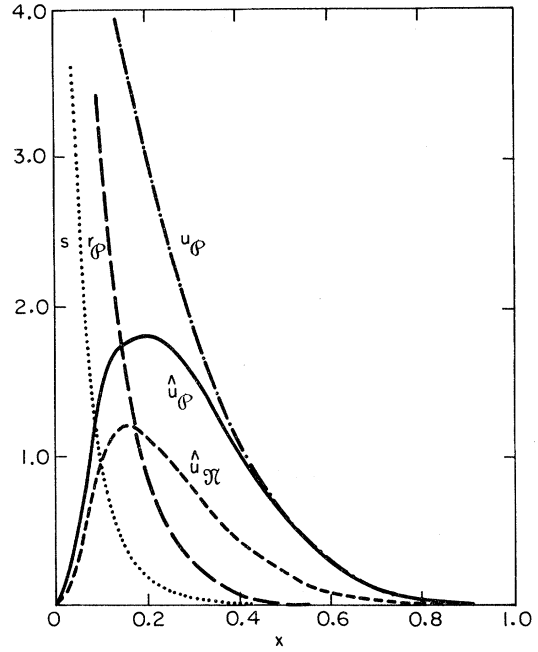


FIG. 4. The parton-distribution functions of Ref. 13.

For  $y = 1 - \tau - \epsilon(1 + \tau)$  and  $\tau = 1 - \epsilon'$ , we obtain a special case of (2.8)

$$\Delta \cong \epsilon^3 \epsilon'^7. \tag{2.8'}$$

So far we have not commented on the  $\vec{Q}_\perp$  dependence of the cross section. In general, the transverse-momentum dependence of the parton-distribution wave functions is not theoretically determined. However, near the threshold region of any given component of one of the  $u_a(x)$ , specific forms of  $\vec{k}_\perp$  dependence can be theoretically motivated. The argument begins with the interchange theory wave-function expression for the given component, call it  $u^c(x)$ , in the region  $x \rightarrow 1$ ,  $k^2 \rightarrow (k_\perp^2 + \sigma)/(1-x) \rightarrow \infty$  [see (1.9)]. In addition the minimal quark number state of limited average core mass squared,  $\bar{\sigma}$ , is expected to dominate. One obtains

$$u^c(x, k^2, \bar{\sigma}) \propto \frac{1}{1-x} \left| \psi^c \left( \frac{k_\perp^2 + \bar{\sigma}}{1-x}, \bar{\sigma} \right) \right|^2, \tag{2.10}$$

where  $\psi^c$  is the wave function describing the breakup of the hadron into parton  $a$  and core  $\bar{\sigma}$ . For example, the natural variable  $k^2$  reduces to a

correlated combination of  $k_{\perp}^2$  and  $1-x$ . The value of  $\bar{\sigma}$  is, of course, uncertain, but probably of the order of 1 GeV<sup>2</sup>. The contribution of this component of the parton's wave function to the proton's spin averaged form factor at momentum transfer  $t = -q_{\perp}^2$  may be written as<sup>6</sup>

$$F^c(q_{\perp}^2) \propto \int \frac{dx}{1-x} d^2k_{\perp} \psi^c \left( \frac{k_{\perp}^2 + \bar{\sigma}}{1-x}, \bar{\sigma} \right) \times \psi^c \left( \frac{[\vec{k}_{\perp} - (1-x)\vec{q}_{\perp}]^2 + \bar{\sigma}}{1-x}, \bar{\sigma} \right). \quad (2.11)$$

Taking

$$\psi^c \propto \left( \frac{k_{\perp}^2 + \bar{\sigma}}{1-x} \right)^{-p_c} \quad (2.12)$$

for large values of  $k_{\perp}^2$ , we find that near  $x=1$ ,

$$u^c(x, k_{\perp}) \propto \frac{(1-x)^{2p_c-1}}{(k_{\perp}^2 + \bar{\sigma})^{2p_c}}, \quad (2.13)$$

$$F^c(q_{\perp}^2) \propto (q_{\perp}^2)^{-p_c} \ln q_{\perp}^2.$$

According to the naive wave-function theory recently developed<sup>13,14</sup> we have the following assignments for  $p_c$ :

$$\begin{aligned} \bar{s}(x) &\leftrightarrow p_c = 4 \quad (\text{5-quark minimal sea state}), \\ r(x) &\leftrightarrow p_c = 4 \quad (\text{5-quark minimal sea state}), \\ \hat{u}_n(x) &\leftrightarrow p_c = \frac{5}{2} \quad (\mathcal{P}\text{-}\mathcal{N} \text{ quark pair member}), \\ \hat{u}_p(x) &\leftrightarrow p_c = 2 \quad (\text{unpaired } \mathcal{P} \text{ quark}). \end{aligned} \quad (2.14)$$

Thus, in the specific situations of (2.8), (2.8'), and (2.9) one should see correlated  $\vec{Q}_{\perp}$  dependence arising from the  $k_{\perp}$  transverse momentum convolution resulting from a  $q\bar{q}$  quark collision

$$\begin{aligned} \frac{d\sigma}{d^2Q_{\perp}} &\propto \frac{d^2k_{\perp}}{(k_{\perp}^2 + \bar{\sigma})^8 [(\vec{Q}_{\perp} - \vec{k}_{\perp})^2 + \bar{\sigma}]^4} \\ &\propto \frac{1}{(Q_{\perp}^2 + \bar{\sigma})^4}. \end{aligned} \quad (2.15)$$

$$\begin{aligned} \Delta^{\pi^+} &= \frac{12}{9} s^{\pi}(x_1) \bar{r}_{\vec{k}_{\perp}} \bar{s}(x_2) \bar{Q}_{\perp} \bar{r}_{\vec{k}_{\perp}} + s^{\pi}(x_1) \bar{r}_{\vec{k}_{\perp}} \left\{ \frac{4}{9} [\hat{u}_{\mathcal{P}}(x_2) + r_{\mathcal{P}}(x_2)] + \frac{1}{9} [\hat{u}_{\mathcal{N}}(x_2) + r_{\mathcal{N}}(x_2)] \right\} \bar{Q}_{\perp} \bar{r}_{\vec{k}_{\perp}} \\ &\quad + [\hat{u}^{\pi}(x_1) + r^{\pi}(x_1)] \bar{r}_{\vec{k}_{\perp}} \left\{ \frac{5}{9} s(x_2) + \frac{1}{9} [\hat{u}_{\mathcal{N}}(x_2) + r_{\mathcal{N}}(x_2)] \right\} \bar{Q}_{\perp} \bar{r}_{\vec{k}_{\perp}}. \end{aligned} \quad (2.19)$$

The corresponding result for  $\pi^-$  is obtained by  $\mathcal{P}\text{-}\mathcal{N}$  quark reflection.

The simple wave-function theories lead to the following expectations<sup>13,14</sup> for  $v^{\pi}$  and  $s^{\pi}$ :

$$\begin{aligned} s^{\pi}(x) &\leftrightarrow p^c = 3 \\ r^{\pi}(x) &\leftrightarrow p^c = 3 \\ \hat{u}^{\pi}(x) &\leftrightarrow p^c = 1 \end{aligned} \left. \begin{array}{l} \left. \begin{array}{l} (4\text{-quark } q\bar{q}q\bar{q} \text{ minimal mesonic} \\ \text{"sea" state}) \\ (q\bar{q} \text{ valence state}). \end{array} \right\} \right. \quad (2.20)$$

For meson-proton collisions, producing a massive

For large enough  $\vec{Q}_{\perp}$  this contribution will no longer dominate; instead, standard high-transverse-momentum processes will take over, which for this case yield<sup>20</sup>

$$\frac{d\sigma}{d^2Q_{\perp} dy d\tau} \propto \frac{1}{Q_{\perp}^4}. \quad (2.16)$$

However, the relatively small difference between (2.16) and (2.15) plus a very much stronger phase-space suppression, for  $y$  or  $\tau$  near unity, associated with (2.16) make it likely that the form (2.15) will be readily observable.

Finally, we note that there are interesting alterations in the above predictions if one of the colliding hadrons is a meson rather than a proton. As an example consider  $\pi^+$  and  $\pi^-$  beams. All the formulas previously given apply except for modifications to (2.1) and (2.7). For  $\pi^+$  distribution functions we expect

$$\begin{aligned} u_{\mathcal{P}}^{\pi}(x) &= v^{\pi}(x) + s^{\pi}(x), \\ u_{\mathcal{N}}^{\pi}(x) &= v^{\pi}(x) + s^{\pi}(x), \end{aligned} \quad (2.17)$$

$$u_{\mathcal{P}}^{\pi} = u_{\mathcal{N}}^{\pi} = u_{\lambda}^{\pi} = u_{\bar{\lambda}}^{\pi} = s^{\pi}.$$

The  $\pi^-$  distribution functions are given by  $q\text{-}\bar{q}$  parton reflection. As in the case of the proton,  $v^{\pi}$  has a Regge component and a valence component,

$$v^{\pi} = \hat{u}^{\pi} + r^{\pi}. \quad (2.18)$$

The lack of pion deep-inelastic scattering data prevents a detailed extraction of these distribution functions. However, threshold behaviors may be determined on theoretical grounds.

Taking the meson to be hadron 1 traveling in the positive  $z$  direction, the analog of (2.7) is

$\mu$  pair, the limits  $y \rightarrow 1 - \tau - \epsilon(1 + \tau)$  and  $y \rightarrow -(1 - \tau) + \epsilon(1 + \tau)$  exhibit quite different behavior. The first limit probes  $x_1 \approx 1$ , where  $\hat{u}^{\pi}$  terms are emphasized, while the second probes  $x_2 \approx 1$ , where  $\hat{u}_p$  terms are prominent. From (2.19) and (2.20) we have

$$\Delta^{\pi^+} \propto \begin{cases} \frac{\epsilon}{Q_{\perp}^4} \frac{1}{9} [\hat{u}_{\mathcal{N}}(\tau) + r_{\mathcal{N}}(\tau) + 5\bar{s}(\tau)], & y \approx (1 - \tau) \\ \frac{\epsilon^3}{Q_{\perp}^8} \frac{4}{9} s^{\pi}(\tau), & y \approx -(1 - \tau) \end{cases} \quad (2.21a)$$

which for  $\tau \rightarrow 1 - \epsilon'$  reduces to

$$\Delta^{\pi^+} \propto \begin{cases} \frac{\epsilon \epsilon'^4}{\bar{Q}_\perp^4}, & y \approx (1 - \tau) \\ \frac{\epsilon^3 \epsilon'^5}{\bar{Q}_\perp^8}, & y \approx -(1 - \tau). \end{cases} \quad (2.21b)$$

We have given the associated  $\bar{Q}_\perp$  dependences in the limit  $\bar{Q}_\perp^2 \gg M^2$ . The  $\epsilon, \epsilon'$  dependences are valid regardless of the  $\bar{Q}_\perp$  value. In particular, these dependences hold for  $\Delta^\pi$  integrated over  $d^2\bar{Q}_\perp$ . The analogous results for  $\pi^-$  would be

$$\Delta^{\pi^-} \propto \begin{cases} \frac{\epsilon}{\bar{Q}_\perp^4} \left[ \frac{1}{9} [4\hat{u}_p(\tau) + 4r_p(\tau) + 5\bar{s}(\tau)] \right], & y \approx (1 - \tau) \\ \epsilon^3 \frac{4}{9} [\hat{u}^\pi(\tau) + r^\pi(\tau) + s^\pi(\tau)]_{\bar{Q}_\perp}, & y \approx -(1 - \tau) \end{cases} \quad (2.22a)$$

which for  $\tau \rightarrow 1 - \epsilon'$  becomes

$$\Delta^{\pi^-} \propto \begin{cases} \frac{1}{9} \frac{\epsilon \epsilon'^3}{\bar{Q}_\perp^4}, & y \approx (1 - \tau) \\ \frac{4}{9} \frac{\epsilon^3 \epsilon'}{\bar{Q}_\perp^4}, & y \approx -(1 - \tau). \end{cases} \quad (2.22b)$$

Note that in the latter case the ratio of  $\Delta^{\pi^-}$  in the two limits is well determined in the quark model and would test the fractional quark charge values.

At  $y=0, \tau \rightarrow 1$  we obtain similarly

$$\begin{aligned} \Delta^{\pi^+} &\rightarrow \frac{1}{9} \hat{u}^\pi(\tau) \hat{u}_n(\tau) \propto \frac{(1 - \tau)^5}{\bar{Q}_\perp^4}, \\ \Delta^{\pi^-} &\rightarrow \frac{4}{9} \hat{u}^\pi(\tau) \hat{u}_p(\tau) \propto \frac{(1 - \tau)^4}{\bar{Q}_\perp^4}. \end{aligned} \quad (2.23)$$

Again the  $1 - \tau$  dependence and the numerical ratio of  $\Delta^{\pi^+}/\Delta^{\pi^-}$  are valid independent of  $\bar{Q}_\perp$  and would test the quark-model wave-function extraction of Ref. 11 in a very clean fashion. We should also note that for the  $\pi$ -induced collisions discussed above, the  $\bar{Q}_\perp$  dependences given will survive even for very large  $\bar{Q}_\perp$  since the direct annihilation processes being considered are the primary contributions in the interchange theory. In contrast, for proton-proton collisions at very large  $\bar{Q}_\perp$ , one of the initial protons tends to create a pion by a bremsstrahlung process; the pion then undergoes a high-transverse-momentum annihilation process resulting in a weaker  $\bar{Q}_\perp$  damping. However, this bremsstrahlung process is very much suppressed<sup>6</sup> near the phase-space boundaries. Thus, the  $\pi$ -meson analog will almost certainly be small compared to the direct production processes in the regions considered.

The results for a  $K^+$  or  $K^-$  beam further illustrate the experimental possibilities. For example, consider the  $y \approx 0, \tau \rightarrow 1$  case. The factor  $\Delta$  becomes

$$\begin{aligned} \Delta^{K^+} &\rightarrow \frac{4}{9} s^\pi(\tau) \hat{u}_\rho(\tau) + \frac{1}{9} \hat{u}^\pi(\tau) \bar{s}(\tau) \\ &\propto (1 - \tau)^3, \end{aligned} \quad (2.24)$$

while

$$\begin{aligned} \Delta^{K^-} &\rightarrow \frac{4}{9} \hat{u}^\pi(\tau) \hat{u}_\rho(\tau) \\ &\propto (1 - \tau)^4. \end{aligned} \quad (2.25)$$

We have used  $K$ -meson quark distribution functions obtained by SU(3) symmetry from the pion ones.

It is perhaps overly optimistic, in view of the present state of the data, to hope for measurements capable of distinguishing these various functional behaviors from one another. However, eventual observation would provide a striking confirmation of the over-all consistency of the parton model. We stress again that even should the model fail for small  $\bar{Q}_\perp$  or for the integral over all  $\bar{Q}_\perp$  (for reasons which may be associated with the difficulties in explaining  $e^+e^-$  annihilation experiments), the model might still hold for  $\bar{Q}_\perp \neq 0$  and should be tested there as well.

### III. COMPARISON WITH EXPERIMENT

In this section we shall present quantitative comparisons with the massive  $\mu$ -pair production data of the Brookhaven-Columbia (BC) collaboration.<sup>13</sup> Before any comparison is possible, consideration must be given to the fact that the energies are not asymptotic and to the experimental aperture limitations.

The highest energy used by the BC group is at  $E_{\text{lab}} = 29.5$  GeV or  $s = 57.2$  GeV<sup>2</sup>. The range of  $\tau$  at asymptotic energies is  $0 < \tau < 1$ ; however, the inclusive cross section must include the production of at least two baryons, so that

$$Q_{\text{max}}^2 = (\sqrt{s} - 2M)^2. \quad (3.1)$$

For  $s = 57.2$  GeV<sup>2</sup>, this gives  $Q_{\text{max}}^2 = 32.3$  (GeV/c)<sup>2</sup>, and so  $\tau_{\text{max}} = 0.565$ . Clearly the effect is substantial.<sup>21</sup>

In Sec. I we developed the techniques needed to account for the subasymptotic kinematic complications to order  $\sqrt{s}$ . Qualitatively, as  $Q^2 \rightarrow Q_{\text{max}}^2$ , the  $\delta$ -function constraint discussed below Eq. (1.17) restricts the distribution-function integrals over  $d^2k_{i\perp}$ ,  $d\sigma_i$ , and  $dx_i$  to a smaller and smaller region of the full phase-space volume. In particular,  $\sigma_i$  is forced to remain near its minimum value  $\sigma_i \sim M^2$  and  $k_{i\perp}$  is forced near zero. These restrictions mean that only a portion of the full distribution-function integral

$$f(x) = \int d^2k_\perp d\sigma f(x, k_\perp^2, \sigma) \quad (3.2)$$

will contribute. The phase-space limitation of the

full  $\delta$  function was implemented in a computer program where the specific choice

$$f(x, k_{\perp}^2, \sigma) = \frac{nM^{2n} \delta(\sigma - M^2)}{\pi(k_{\perp}^2 + M^2)^{n+1}} f(x) \quad (3.3)$$

was used. This particular factorized form for  $f(x, k_{\perp}^2, \sigma)$  is significant only inasmuch as it is a convenient and reasonable method for quantifying the phase-space limitation. One should be cautious in accepting this as a complete treatment of the threshold region because other diagrams more complicated than the one considered might become important. The powers  $n$  are chosen in accordance with the theoretical results of Sec. II.

$$W_E(\tau) = \int_0^1 dx_1 \int_0^1 dx_2 \Theta\left(x_1 - \frac{2Mq_{L\min}}{s}\right) d^2k_{1\perp} d^2k_{2\perp} \delta((k_1 + k_2)^2 - Q^2) s x_1 x_2 \sum_a \lambda_a^2 f_a(x_1, k_{1\perp}^2) f_a^-(x_2, k_{2\perp}^2), \quad (3.5)$$

with

$$(k_1 + k_2)^2 = x_1 x_2 (s - 2M^2) - \frac{x_1^2 M^2}{1 - x_1} - \frac{x_2^2 M^2}{1 - x_2} - \frac{\vec{k}_{1\perp}^2}{1 - x_1} - \frac{\vec{k}_{2\perp}^2}{1 - x_2}. \quad (3.6)$$

A comparison with the data of the Brookhaven-Columbia experiment for  $E_{\text{lab}} = 29.5$  GeV ( $s = 57.2$  GeV<sup>2</sup>) is shown in Fig. 5. The lower dashed curve is the prediction of the model without the threshold effects due to the kinematic limitation in  $Q^2$ . The lower solid curve is the prediction with threshold effects. Both curves include the Drell-Yan accommodation to the experimental aperture ( $q_{L\min} \geq 12$  GeV/c in the lab). Also shown are the model predictions at energies typical of the ISR at CERN,  $s = 900$  GeV<sup>2</sup> and  $s = 2500$  GeV<sup>2</sup>. At these energies, the threshold effect is negligibly small.

The total cross section as a function of energy is shown in Fig. 6. The dashed curve is the model prediction without threshold effects and the solid curve is the prediction with threshold effects. The cross section lies between five and six times lower than the experimental measurements. Giving the quarks "color," in an SU(3) color group,<sup>22</sup> which seems to be required to explain the  $\pi^0 \rightarrow 2\gamma$  decay rate, decreases the cross section everywhere by a factor of 3, making the over-all normalization even worse. It is apparent that inclusion of the threshold effect greatly increases the energy dependence of the total cross section over the range of Brookhaven energies, although the increase is still not quite as sharp as the experiment indicates.

One may ask if the distribution functions used

The constraints dictated by the experimental apparatus precluded the detection of many events leading to a lepton pair of squared mass  $Q^2$ . Only events with longitudinal momentum  $q_L \geq 12$  GeV/c in the lab and with  $|\vec{Q}_{\perp}|/|\vec{Q}| \leq \frac{1}{16}$  were observed. We follow the procedure of Drell and Yan<sup>7</sup> for taking this cut into account by introducing a  $\Theta$  function in the  $dx_1 dx_2$  integrations.

Thus, the differential cross section for comparison with experiment is

$$\left(\frac{d\sigma}{dQ^2}\right)_E = \frac{4\pi\alpha^2}{3Q^2} \frac{1}{Q^2} \tau W_E(\tau), \quad (3.4)$$

where

here may be modified in some way such that the fit to  $d\sigma/dm_{\mu\mu}$  is improved. In particular, the detailed shape of the parton prediction is very sensitive to the functional form chosen for the sea

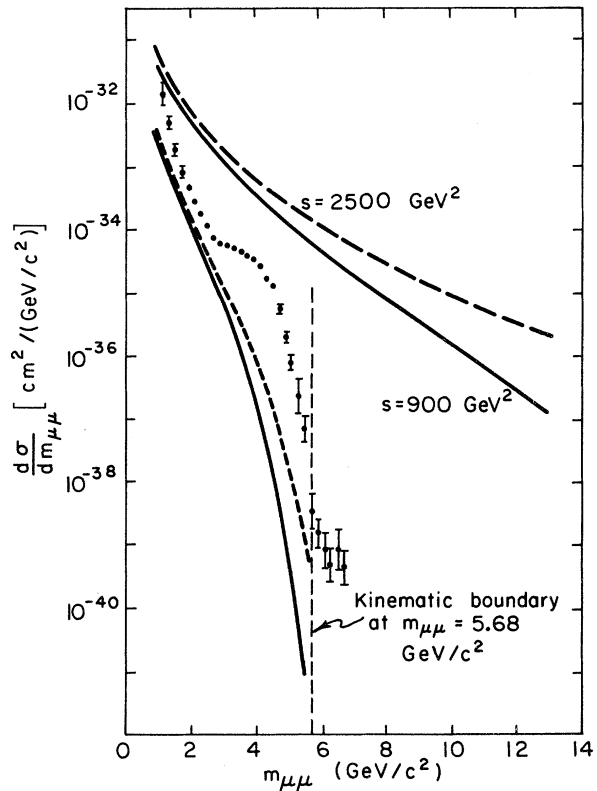


FIG. 5. The comparison with data. The lower dashed curve indicates the prediction ignoring the kinematical limitation in  $m_{\mu\mu}$ . The lower solid curve is the prediction with our accommodation. Also shown are predictions for typical ISR energies.



distribution  $\bar{s}(x)$ . Of course, any modification must be consistent with positivity of the  $\hat{u}$  components, the electroproduction data (2.3), the neutrino data (2.6), the usual quantum-number sum rules (2.5), and the requirements that  $\bar{s}(x) \propto 1/x$  as  $x \rightarrow 0$ , and that  $\bar{s}(x) \propto (1-x)^7$  as  $x \rightarrow 1$ .

We have experimented with functional forms for the sea of the form

$$\bar{s}(x) = a_n (1-x)^7/x + b_n x^n (1-x)^7 \quad (3.7)$$

for various values of  $n$ ,  $a_n$ ,  $b_n$ . The best fit consistent with the constraints listed above occurs for  $n=4$ ,  $a_n=0.15$ ,  $b_n=75$ . For any given form of  $\bar{s}(x)$  the remaining distribution-function components may be recomputed from the deep-inelastic data and the sum rules following the methods of Ref. 13; for the above choice we obtain

$$r_\phi(x) = 2.420(1-x)^7/\sqrt{x},$$

$$r_{\mathcal{N}}(x) = 1.555(1-x)^7/\sqrt{x},$$

and the  $\hat{u}$  curves plotted in Fig. 7. The changes in  $u_\phi(x)$  and  $u_{\mathcal{N}}(x)$  are for the present purpose relatively insignificant. The most significant change occurs in  $s(x)$ , which becomes much larger than the old sea distribution for  $x > 0.3$ . The resultant curve for  $d\sigma/dm_{\mu\mu}$  is shown as the dashed line in Fig. 8. The trace of a shoulder appears for  $m_{\mu\mu}$  between 2 and 4 GeV/c<sup>2</sup>. However, although the improvement is substantial, it is not large enough to reproduce the pronounced shoulder of the data.

It does not appear possible that allowable modifications to the sea distribution (with consequent modifications to the other distribution components) as in (3.7) can generate either the shape or the normalization of the experimental points. The constraints on the parton model imposed by the data from electroproduction, neutrino scattering, and large-angle scattering are quite severe, and leave little room for freedom. In particular, these data imply that for  $x > 0.2$  the distributions for the sea partons become very small relative to the valence partons.

The most recent neutrino data from FNAL lead to the following additional sum rules<sup>23</sup> which constrain the sea distributions  $s$  and  $s'$  still further:

$$\int dx 2x [u_{\bar{\phi}} + u_{\mathcal{N}}] = 0.052 \pm 0.024, \quad (3.8)$$

$$\int dx \frac{2}{3} x [u_\lambda + u_\chi + 4u_\phi + 4u_{\bar{\phi}}] = 0.14 \pm 0.10.$$

Reference 23 included the possibility of "charmed" quarks and antiquarks,  $\phi'$  and  $\bar{\phi}'$ , in the sea. If, for simplicity, we assume that  $u_{\phi'} = u_{\bar{\phi}'} = 0$ , then the sea distributions strongly violate SU(3) symmetry,

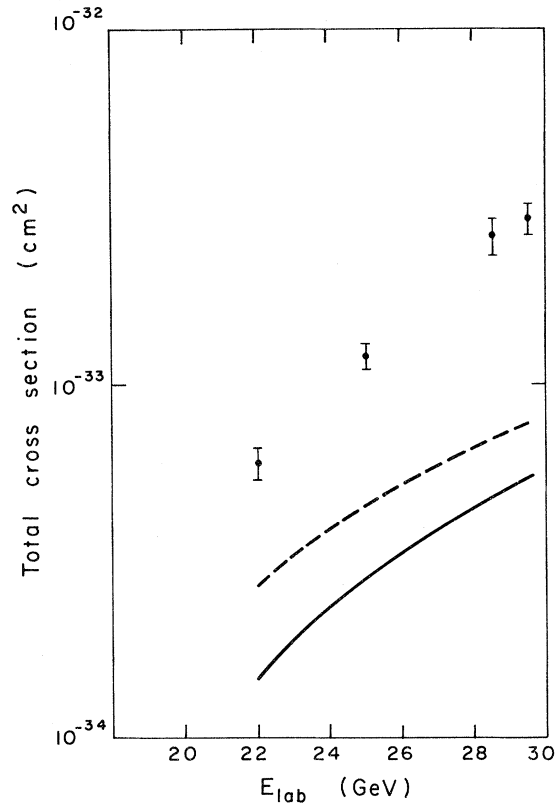


FIG. 6. The total cross section. The dashed curve is the prediction ignoring the kinematical limitation and the solid curve is the prediction taking it into account.

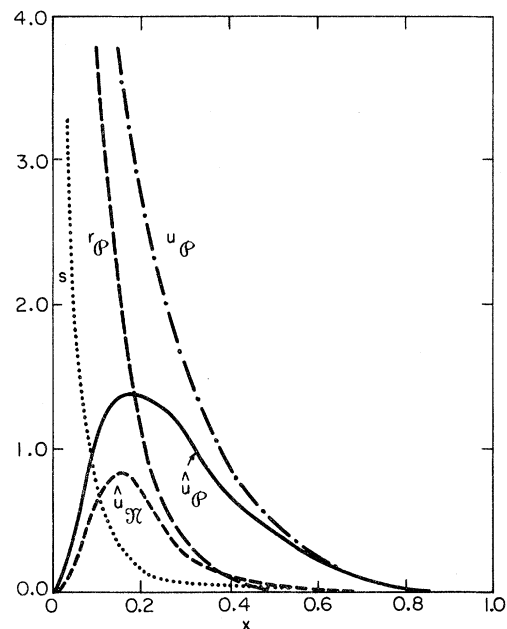


FIG. 7. The parton-distribution functions generated by improving the "sea" as much as is allowed by the data from experiments other than  $\mu$ -pair production.

$$\begin{aligned} s(x) &\approx \frac{1}{2} \bar{s}(x), \\ s'(x) &\approx 4\bar{s}(x), \end{aligned} \quad (3.9)$$

and the fit to the data becomes a little worse. The results are shown in Fig. 8 as the dot-dashed curve. Of course, if the charmed quarks are included in the sum rules, both SU(3) and SU(4) are broken more gently. However, the results are essentially unchanged.

Clearly the pronounced shoulder in the  $d\sigma/dm_{\mu\mu}$  distribution is not predicted. Previously, use of naive distribution functions<sup>7</sup> indicated the possibility of a weak falloff for  $d\sigma/dm_{\mu\mu}$  with increasing  $m_{\mu\mu}$ , as characterized by the shoulder. However, it is clear that the more realistic distribution functions, for which antiquarks have higher threshold damping than quarks, combined with the threshold effect have eliminated this possibility.

Inclusion of a Pomeron contribution as suggested by Landshoff and Polkinghorne<sup>9,24</sup> will not alter this conclusion. For small  $\tau$ , the Pomeron contribution has the same  $\tau$  behavior as the parton-antiparton process, while it vanishes still more rapidly as  $\tau$  grows large. We have chosen to ignore it in the present analysis though one should keep in mind that its presence may, in part, explain the definite discrepancy between the experimental data and the parton prediction in the small- $\tau$  region.

The possibilities that either two-photon processes<sup>25</sup> or radiative corrections<sup>26</sup> may be significant have been ruled out. At Brookhaven energies such terms can change  $d\sigma/dm_{\mu\mu}$  by less than 0.1%.

Inspection of Figs. 5 and 8 shows that the data begin a dramatic departure from the parton predictions at  $Q^2 \approx 10$  (GeV/c)<sup>2</sup>. The same effect occurs at  $E_{\text{lab}} = 22, 25,$  and  $28.5$  GeV, always near the same point in  $Q^2$ . It is interesting to note that in the electron-positron colliding beam experiment, the cross section begins a sharp rise over the parton colored-quark prediction also at  $Q^2 \approx 10$  (GeV/c)<sup>2</sup>.<sup>10,11</sup>

West has recently suggested that such a rise may be explained by endowing the parton with a form factor and an anomalous magnetic moment in such a way that agreement with the electroproduction data is preserved.<sup>12</sup> The parton-photon interaction vertex is modified to

$$\lambda_a e \gamma^\mu \rightarrow \lambda_a e [\gamma^\mu F_1^a(Q^2) + i \sigma^{\mu\nu} Q_\nu \mu_a F_2^a(Q^2)], \quad (3.10)$$

where  $\mu_a$  is the anomalous magnetic moment in units of twice the parton mass. The form factors are given by

$$F_1^a(Q^2) = F_2^a(Q^2) = \frac{1}{1 - Q^2/\Lambda^2}. \quad (3.11)$$

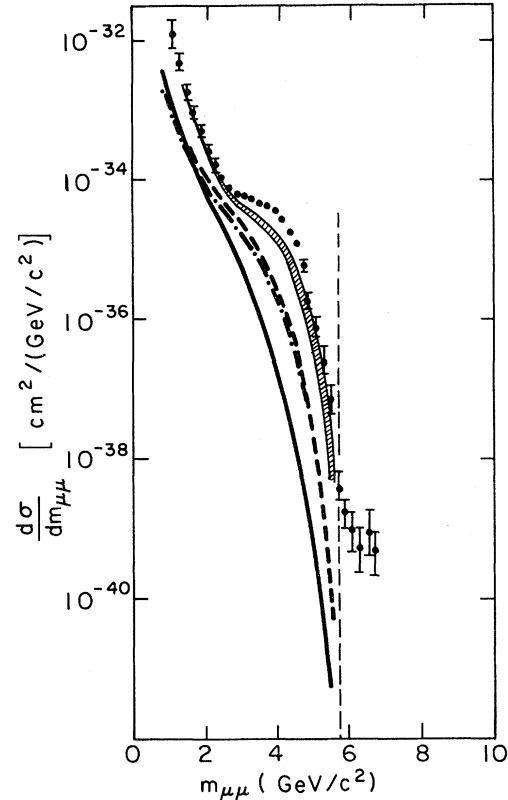


FIG. 8. More comparisons with the data. The solid curve comes from the unmodified distribution functions used in Fig. 5. The dashed curve is the result using the "improved" sea distribution. The dot-dashed curve is the result using both the new sea and the strong SU(3) breaking implied by the neutrino data. The shaded area is the result of renormalizing the data by factoring out the parton form factor and anomalous magnetic moment as suggested by West (Ref. 12).

West finds agreement with both the electroproduction and annihilation data for values

$$\Lambda \approx 8-10 \text{ GeV}, \quad (3.12)$$

$$\mu_a \approx 0.1-0.2 \text{ GeV}^{-1}.$$

Substituting the new vertex in the calculation for the  $\mu$ -pair production cross section [Eqs. (1.10) through (1.14)] yields the change

$$d\sigma \rightarrow d\sigma \left( \frac{1}{1 - Q^2/\Lambda^2} \right)^2 \left( 1 + \frac{\mu^2 Q^2}{4} \right). \quad (3.13)$$

This multiplicative factor has a significant rise with  $Q^2$  for values of  $Q^2 < \Lambda^2$ . We have divided the data by this parton structure factor to show a curve which might presumably represent the "scaling" portion of the  $d\sigma/dm_{\mu\mu}$  distribution. The shaded area in Fig. 8 represents the possible limits for the choice of parameters in (3.12). It

is worth noting that although the normalization is wrong, the *shape* of the distribution as generated by the modified sea distribution (3.7) is not so different from the shape of the "scaling" portion of the experimental curve. The shoulder is still not fully reproduced, however.

Finally, we can give reasonably exact results for the longitudinal momentum distribution of the  $\mu$  pair in proton-proton scattering. Neglecting terms of order  $Q_{\perp}^2/s$ , the cross section is

$$d\sigma \cong \frac{4\pi\alpha^2}{3s} \frac{1}{\tau(y^2+4\tau)^{1/2}} \sum_a \lambda_a^2 f_a(x_{\perp}) f_{\bar{a}}(x_2) dy d\tau, \quad (3.14)$$

with

$$x_{1,2} = \frac{\pm y + (y^2 + 4\tau)^{1/2}}{2}.$$

The cross section is plotted as a function of  $y$  for different values of  $\tau$  in Fig. 9.

We can make a comparison with the BC experiment by integrating over  $\tau$  for the experimental aperture  $Q^2 > 1$  ( $\text{GeV}/c$ )<sup>2</sup>. The kinematical limitation on  $Q_{\text{max}}^2$  is unimportant since less than 1% of the cross section comes from the region  $\tau > 0.3$ . The results are shown as the solid curve in Fig. 10. We have used the distributions of (2.2) without modifications for the sea. The dot-dashed curve shows the distribution renormalized by a constant factor to the experimental curve. Thus it can be seen that the shape of the parton prediction agrees closely with experiment over four decades. The dashed curve is the parton prediction using the crude distributions of Drell and Yan.<sup>7</sup> Again, the fit is remarkable, even though their distributions are identical for all species of partons and antipartons. Of course, the major contribution to the cross section in Fig. 10 comes from the small- $\tau$  region, where Pomeron  $1/x$  behavior dominates and the approximations made by Drell and Yan are not critical. It would be possible to resolve the details of the parton distributions by taking cuts in the data for larger  $Q^2$  (i.e.,  $\tau$ ), as discussed in Sec. II.

### CONCLUSIONS

It is clear from our analysis that the usual parton-antiparton annihilation process cannot explain the magnitude of the cross section for  $\mu$ -pair production at Brookhaven energies. If we give the quarks color and if we believe the results of the neutrino experiments for the antiquark distributions, then our predictions fall almost a factor of 20 below the experimental cross section. (The situation is even getting slightly worse with increasing energy, as shown in Fig. 6.)

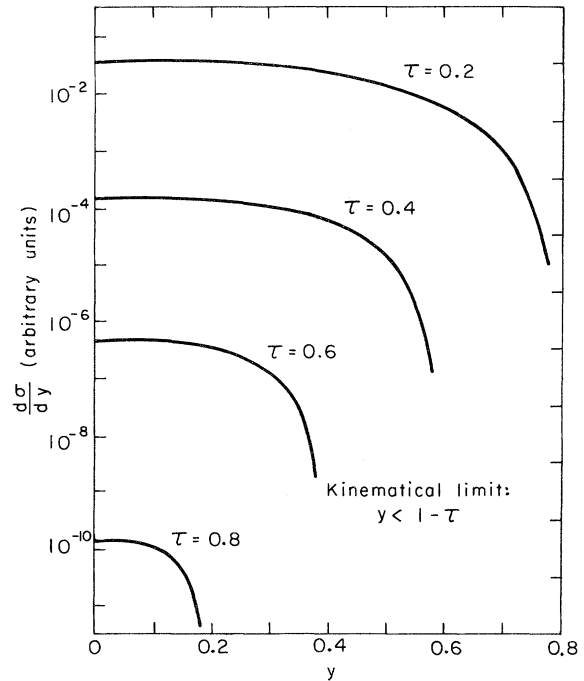


FIG. 9. The longitudinal momentum distribution of the  $\mu$  pair for various values of  $\tau$  as predicted by the model.

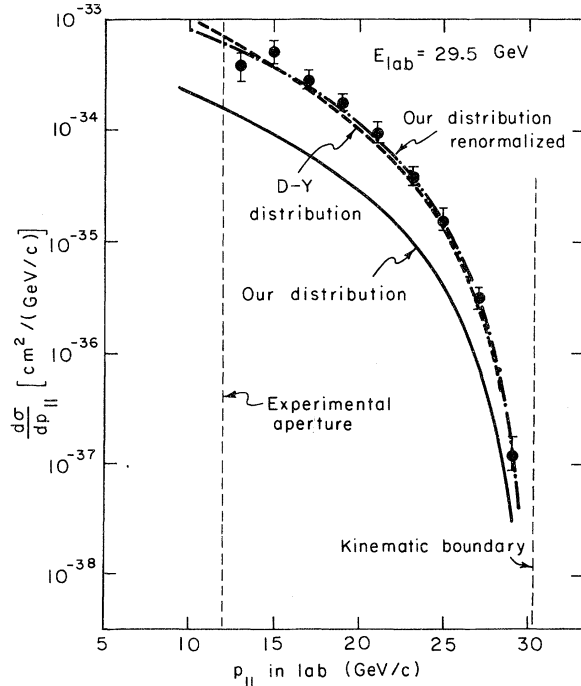


FIG. 10. The longitudinal momentum distribution of the  $\mu$  pair as seen in the lab. The solid curve is our prediction; the dot-dashed curve is our prediction renormalized to the total cross section, to compare its shape to the data; the dashed curve is the Drell-Yan prediction, normalized to the total cross section.

One may speculate that the discrepancy may be explained by a large diffractive component.<sup>9,24</sup> But precise quantitative predictions have not yet been made.

We note here that our fit to the data is significantly worse than that made by previous authors using naive versions of the quark-parton model.<sup>7-9</sup> The reason is threefold: (1) We have demanded consistency with the neutrino data; (2) the sea distributions reflect the severely damped threshold behavior consistent with large-angle scattering theory; (3) we have taken into account the kinematic limitations imposed by the subasymptotic energy of the BC experiment.

We have seen that the shape of the longitudinal momentum distribution of the  $\mu$  pair is (perhaps accidentally) reproduced by the parton model, at least for the cut in the data given by the BC experiment.

Furthermore, the approximate shape of the invariant mass distribution  $d\sigma/dm_{\mu\mu}$  and, in particular, the pronounced shoulder beginning at  $Q^2 \approx 10$  (GeV/c)<sup>2</sup> may be generated by a parton model, if the partons are given a form factor and an anomalous magnetic moment. [Even if one does not believe in such an explanation, the shoulder may, in fact, be related to the unexpected rise above  $Q^2 \approx 10$  (GeV/c)<sup>2</sup> observed in the electron-positron annihilation experiments.] However, since the parton structure corrections fail to reproduce the normalization of the Brookhaven data, this must be regarded as no more than a curiosity.

Nonetheless the parton model may be valid for a restricted region of phase space, perhaps for larger transverse momentum, or in the region near the phase-space boundaries. The observation of large- $Q_{\perp}$  events enhances the likelihood of its applicability, in view of the successes of high-transverse-momentum parton phenomenology even in hadron physics.

One may speculate further, and wonder whether the usual quark charge assignments are wrong,

and therefore responsible for the difficulties in normalization. Perhaps, there is simply a large nonscaling piece to the cross section which has not yet disappeared at Brookhaven energies. However, such a piece would have to be considerably larger than most parton enthusiasts would be willing to endure.

It is safe to say that the conclusion of our study is that the usual quark-parton mechanism for  $\mu$ -pair production has serious difficulty in explaining the Brookhaven-Columbia experiment.

In any case, future experiments at higher energies and with enough resolution to probe all regions of phase space are eagerly awaited.

*Note added in proof.* After the completion of our work on this paper, we received reports from Einhorn and Savit<sup>27</sup> and from Paar and Paschos<sup>28</sup> which also studied the difficulties of the parton model in explaining the Brookhaven data. They also conclude that the parton predictions fall significantly below the data.

We also received a report from Goldman and Vinciarelli<sup>29</sup> which considers the possibility that the shoulder in the  $\mu$ -pair cross section may be related to the rise in the  $e^+e^-$  annihilation cross section. Our approach was to attempt to answer the question by introducing structure to the partons, while their approach was more general.

Recently, Henyey and Savit<sup>30</sup> have studied the diffractive final-state interaction proposed by Landshoff and Polkinghorne.<sup>9,24</sup> They have shown that when such a diagram is added to the usual Drell-Yan mechanism, the cross section *decreases*.

#### ACKNOWLEDGMENTS

The authors would like to acknowledge the hospitality of the Center for Theoretical Physics at MIT where this work was begun. They also thank M. Suzuki, S. Brodsky, D. Jackson, and H. Stapp for helpful conversations.

\*This work was supported in part by the U. S. Atomic Energy Commission.

<sup>1</sup>See R. P. Feynman, *Photon Hadron Interactions* (Benjamin, New York, 1972).

<sup>2</sup>E. D. Bloom *et al.*, MIT-SLAC Report No. SLAC-PUB-796, 1970 (unpublished), presented at the Fifteenth International Conference on High Energy Physics, Kiev, U.S.S.R., 1970.

<sup>3</sup>J. J. Sakurai, *Phys. Rev. Lett.* **22**, 981 (1969).

<sup>4</sup>R. A. Brandt, *Phys. Rev. Lett.* **23**, 1260 (1969); B. L. Ioffe, *Phys. Lett.* **30B**, 123 (1969); R. A. Brandt, *Phys. Rev. D* **1**, 2808 (1970); G. Altarelli, R. A. Brandt, and G. Preparata, *Phys. Rev. Lett.* **26**, 42 (1971).

<sup>5</sup>S. D. Drell, D. Levy, and T.-M. Yan, *Phys. Rev. D* **1**, 1617 (1970).

<sup>6</sup>For a review see J. F. Gunion, in proceedings of the International Symposium on Multiparticle Hadrodynamics, Pavia, 1973 (unpublished); S. J. Brodsky, in *High Energy Collisions—1973*, proceedings of the fifth international conference on high energy collisions, Stony Brook, 1973, edited by C. Quigg (A.I.P., New York, 1973).

<sup>7</sup>S. D. Drell and T.-M. Yan, *Ann. Phys. (N.Y.)* **66**, 578 (1971).

<sup>8</sup>J. Kuti and V. Weisskopf, *Phys. Rev. D* **4**, 3418 (1971).

<sup>9</sup>P. Landshoff and J. C. Polkinghorne, *Nucl. Phys.* **B33**,

- 221 (1971).
- <sup>10</sup>A. Litke *et al.*, Phys. Rev. Lett. **23**, 1196 (1973), and references therein.
- <sup>11</sup>B. Richter, invited talk at the Irvine Conference, 1974 (unpublished).
- <sup>12</sup>G. West, Stanford University report, 1974 (unpublished); M. Chanowitz and S. Drell, Phys. Rev. D **9**, 2078 (1974).
- <sup>13</sup>J. F. Gunion, Phys. Rev. D **10**, 242 (1974).
- <sup>14</sup>G. Farrar, Nucl. Phys. **B77**, 429 (1974); R. Blankenbecler, S. Brodsky, and J. Gunion, Phys. Lett. **39B**, 649 (1972); Phys. Rev. D **8**, 287 (1973); S. Brodsky and G. Farrar, Phys. Rev. Lett. **31**, 1153 (1973).
- <sup>15</sup>J. H. Christenson *et al.*, Phys. Rev. D **8**, 2016 (1973).
- <sup>16</sup>S. Brodsky, F. Close, and J. F. Gunion, Phys. Rev. D **8**, 3678 (1973). See also P. V. Landshoff, J. C. Polkinghorne, and R. Short, Nucl. Phys. **B28**, 225 (1971) for the Sudakov approach.
- <sup>17</sup>In general, subtraction terms are present, which insure the convergence of the integral. It is shown in Ref. 16 that they contribute only to the real part of  $T_a$ . It happens that only the imaginary part of  $T_a$  contributes to  $W^{\mu\nu}$ , so the subtraction terms do not affect our calculation.
- <sup>18</sup>S. D. Drell and T.-M. Yan, Phys. Rev. Lett. **24**, 131 (1970); G. West, *ibid.* **24**, 1206 (1970).
- <sup>19</sup>D. H. Perkins, in *Proceedings of the XVI International Conference on High Energy Physics, Chicago-Batavia, Ill., 1972*, edited by J. D. Jackson and A. Roberts (NAL, Batavia, Ill., 1973), Vol. 4, p. 189. Although the Gargamelle data are at relatively low energy ( $E_\nu = 1$  to 5 GeV), there is some evidence for precocious scaling in that the  $\nu$  and  $\bar{\nu}$  total cross sections seem to rise linearly and are consistent with the NAL results. T. Eichten *et al.* (Gargamelle), Phys. Lett. **46B**, 274 (1973); A. Benvenuti *et al.* (NAL), Phys. Rev. Lett. **22**, 125 (1974).
- <sup>20</sup>J. F. Gunion, S. J. Brodsky, and R. Blankenbecler, work in preparation.
- <sup>21</sup>We are indebted to M. Suzuki for emphasizing the importance of this elementary fact.
- <sup>22</sup>W. A. Bardeen, H. Fritzsch, and M. Gell-Mann, in *Scale and Conformal Symmetry in Hadron Physics*, edited by R. Gatto (Wiley-Interscience, New York, 1973), p. 139.
- <sup>23</sup>A. DeRújula, H. Georgi, S. Glashow, and H. Quinn, Rev. Mod. Phys. **46**, 391 (1974).
- <sup>24</sup>P. V. Landshoff and J. C. Polkinghorne, Nucl. Phys. **B36**, 642E (1972).
- <sup>25</sup>A. Soni, Phys. Rev. D **8**, 880 (1973).
- <sup>26</sup>A. Soni, Phys. Rev. D **8**, 2264 (1973).
- <sup>27</sup>M. Einhorn and R. Savit, Phys. Rev. D **10**, 2785 (1974); NAL Report No. NAL-Pub-74/41-THY, 1974 (unpublished).
- <sup>28</sup>H. Paar and E. Paschos, Phys. Rev. D **10**, 1502 (1974).
- <sup>29</sup>T. Goldman and P. Vinciarelli, Phys. Rev. D (to be published).
- <sup>30</sup>F. Henyey and R. Savit, NAL Report No. NAL-Pub-74/29-THY, 1974 (unpublished).

## Quark pairing and elastic scattering at large momentum transfer

J. F. Gunion

*Department of Physics, University of Pittsburgh, Pittsburgh, Pennsylvania 15260*

(Received 20 May 1974)

We reassess interchange-theory predictions for elastic meson-baryon and baryon-baryon reactions in light of the apparent quark pairing within the proton. The theoretical forms are compared to existing data.

This paper is intended as a reassessment of interchange-theory<sup>1,2</sup> predictions for elastic meson-baryon reactions—though some consideration is also given to baryon-baryon scattering. We will give the alterations to the original interchange results that must be incorporated in light of the apparent quark pairing<sup>3</sup> within the proton (responsible for  $F_2^{\text{en}}/F_2^{\text{ep}} \rightarrow \frac{1}{3}$  as  $\omega \rightarrow 1$ ). Experimental comparisons are made, with particular emphasis upon 90° cross-section ratios for available processes related by SU(3). The value of precise experimental measurements of these as a test of the theory

is emphasized. Remarkably, current data, despite their low energy ( $P_{\text{lab}} \sim 10$  GeV/c), are found to be consistent with interchange-theory predictions, with one exception.

The theoretical forms for elastic meson-baryon reactions are easily obtained. We employ covariant formalism and outline a calculation of the standard (*ut*) topology diagram (Fig. 1) using a particularly convenient technique.<sup>4</sup> The purpose of this exercise is to emphasize the “nuclear”-physics-like result for the scattering amplitude. We employ a  $P \rightarrow \infty$  frame (see Fig. 1),